Simultaneous use of Cs and Rb Rydberg atoms for dipole moment assessment and RF electric field measurements via electromagnetically induced transparency

Matt T. Simons, Joshua A. Gordon, and Christopher L. Holloway

Articles you may be interested in

Using frequency detuning to improve the sensitivity of electric field measurements via electromagnetically induced transparency and Autler-Townes splitting in Rydberg atoms
Appl. Phys. Lett. **108**, 174101 (2016); 10.1063/1.4947231

Millimeter wave detection via Autler-Townes splitting in rubidium Rydberg atomsa)
Appl. Phys. Lett. **105**, 024104 (2014); 10.1063/1.4890094

Sub-wavelength imaging and field mapping via electromagnetically induced transparency and Autler-Townes splitting in Rydberg atoms
Appl. Phys. Lett. **104**, 244102 (2014); 10.1063/1.4883635

Laser frequency offset locking using electromagnetically induced transparency
Appl. Phys. Lett. **90**, 171120 (2007); 10.1063/1.2734471

Dynamics of autoionizing Rydberg atoms in an electric field
AIP Conf. Proc. **477**, 197 (1999); 10.1063/1.59357

Simultaneous use of Cs and Rb Rydberg atoms for dipole moment assessment and RF electric field measurements via electromagnetically induced transparency

Matt T. Simons, Joshua A. Gordon, and Christopher L. Holloway[a)]

National Institute of Standards and Technology (NIST), Electromagnetics Division,
U.S. Department of Commerce, Boulder Laboratories, Boulder, Colorado 80305, USA

We demonstrate simultaneous electromagnetically-induced transparency (EIT) with cesium (Cs) and rubidium (Rb) Rydberg atoms in the same vapor cell with coincident (overlapping) optical fields. Each atomic system can detect radio frequency (RF) electric (E) field strengths through the modification of the EIT signal (Autler-Townes (AT) splitting), which leads to a direct International System of Unit traceable RF E-field measurement. We show that these two systems can detect the same RF E-field strength simultaneously, which provides a direct *in situ* comparison of Rb and Cs RF measurements in Rydberg atoms. In effect, this allows us to perform two measurements of the same E-field strength, providing a relative comparison of the dipole moments of the two atomic species. This gives two measurements that help rule out systematic effects and uncertainties in this E-field metrology approach, which are important when establishing an international measurement standard for an E-field strength, and is a necessary step for this method to be accepted as a standard calibration technique. We use this approach to measure E-fields at 9.2 GHz, 11.6 GHz, and 13.4 GHz, which correspond to three different atomic states (different principal atomic numbers and angular momentums) for the two atom species. [http://dx.doi.org/10.1063/1.4963106]

I. INTRODUCTION

A stated goal of international metrology organizations and National Metrology Institutes (NMIs), including the National Institute of Standards and Technology (NIST), is to make all measurements directly traceable to the International System of Units (SI). Whenever possible, we would like these metrology techniques to be able to make an absolute measurement of a physical quantity of interest plus any measurement based on the atom to provide a direct SI traceability path and hence enable absolute measurements of physical quantities. Measurement standards based on atoms have been used for a number of years for a wide array of applications; most notable are time, frequency, and length. There is a need to extend these atom-based techniques to other physical quantities, such as electric (E) fields. In recent work, we (and others) have demonstrated a fundamentally new approach for self-calibrated SI-traceable E-field measurements with the capability of fine spatial resolution (including sub-wavelength resolution).[1–5]

This new approach utilizes the concept of electromagnetically induced transparency (EIT).[1,2,6] Consider a sample of stationary four-level atoms illuminated by a single weak ("probe") light field, as depicted in Fig. 1. In this approach, one laser is used to probe the response of the atoms and a second laser is used to excite the atoms to a Rydberg state (the coupling laser). In the presence of the coupling laser, the atoms become transparent to the probe laser transmission (this is the concept of EIT). The coupling laser wavelength is chosen such that the atom is at a high enough principle-quantum

state such that a radio frequency (RF) field can cause an atomic transition. The RF transition in this four-level atomic system causes Autler-Townes (AT) splitting of the transmission spectrum (the EIT signal) for a probe laser. This splitting of the probe laser spectrum is easily measured and is directly proportional to the applied RF E-field amplitude (through Planck's constant and the dipole moment of the atom). By measuring this splitting, we can directly measure the RF E-field strength with the following:[1]

$$|E| = 2\pi \frac{\hbar}{\wp} \frac{\lambda_p}{\lambda_c} \Delta f_m = 2\pi \frac{\hbar}{\wp} \Delta f_o, \tag{1}$$

where Δf_m is the measured splitting, $\Delta f_o = \frac{\lambda_p}{\lambda_c} \Delta f_m$, $\hbar$ is Planck's constant, and $\wp$ is the atomic dipole moment of the RF transition. The ratio $\frac{\lambda_p}{\lambda_c}$ (where λ_p and λ_c are the wavelengths of the probe and coupling lasers, respectively) accounts for the Doppler mismatch of the probe and coupling lasers.[6] We consider this type of measurement of the E-field strength a direct SI-traceable self-calibrated measurement in that it is related to Planck's constant (which will become an SI-defined quantity by standard bodies in the near future) and only requires a frequency measurement (Δf_m, which can be measured very accurately). A typical measured EIT signal from this technique is shown in Fig. 2 for the case with and without RF applied. The experimental setup and details are given below. Application of RF (via a horn antenna placed 318 mm from the vapor cell) at 13.404 GHz couples two high laying Rydberg states and splits the EIT peak as shown in the solid curve in the figure. We measured the AT splitting (Δf_m) of the EIT signal in the probe spectrum for a range of RF source levels and determine the E-field amplitude using (1). These values are also shown in the figure.

[a)]holloway@boulder.nist.gov
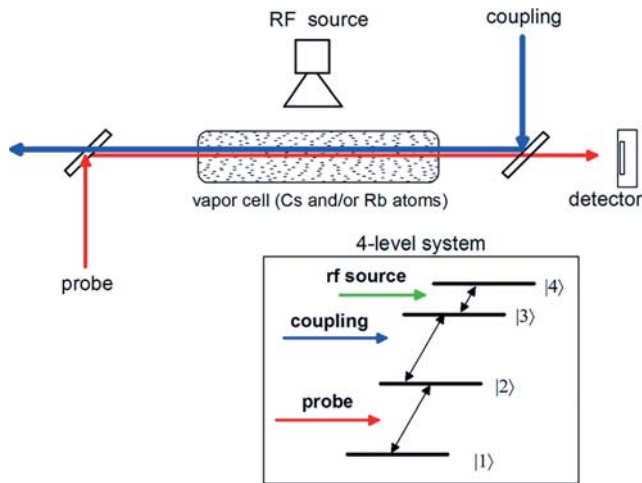
     120, 123103-1

FIG. 1. Illustration of a four-level system, and the vapor cell setup for measuring EIT, with counter-propagating probe and coupling beams. The RF is applied transverse to the optical beam propagation in the vapor cell.

The uncertainties of these types of measurements are currently being investigated.[1,7,8] With that said, for a new measurement method to be accepted by NMIs, the accuracy of the approach must be assessed. By performing simultaneous EIT measurements with two different atomic species in the same vapor cell with coincident (overlapping) optical fields exposed to the identical E-field, we can assess various aspects of the technique. There are subtle aspects of this technique that using two different atoms allows us to address and perform such dual atom experiments help in understanding systematic effects and uncertainties of this approach. For example, these experiments will help in assessing the accuracy of the relative dipole moment calculations of the various atoms in thermal vapor cells at room temperature. One significant source of uncertainty for this measurement approach is the perturbation of the RF field by the vapor

cell.[1,3,7,8] While reducing the effects of the vapor cell on these measurements is an area of active research,[7,8] the experiments in this paper were designed to measure the field at the same location in the cell, not investigate the field variability effects. By preparing two independent atomic systems in the same location of the same vapor cell, we can eliminate the field variability due to the cell when comparing our measurements. As such, the field variability in the vapor cell does not affect the results of these dual atom measurements. This allows us to perform the two measurements of the same field strength, proving a relative comparison of the dipole moment of the two atomic species. In this paper, we demonstrate simultaneous E-field measurement via EIT using both cesium atoms (^{133}Cs) and rubidium-85 (^{85}Rb) atoms in the same vapor cell. We discuss various aspects of these coincident tests by measuring E-fields in the 9.2 GHz, 11.6 GHz, and 13.4 GHz frequency range.

II. RF TRANSITIONS FOR Cs AND Rb

The broadband nature of this technique is due to the large number of possible Rydberg states that can exhibit a large response to an RF source.[1] In order to perform these types of simultaneous measurements, we need to choose states for ^{133}Cs and ^{85}Rb that have similar RF transition frequencies. While there are a large number of possible atomic states with RF transition frequencies, several of these have small atomic dipole moments. Since the measurement splitting (Δf_m) is directly proportional to the atomic dipole moments, we need to use RF transitions with large dipole moments. The four classes of RF transitions corresponding to $nD_{5/2}$–$(n+1)P_{3/2}$, $nD_{5/2}$–$(n-1)F_{7/2}$, $nS_{1/2}$–$nP_{3/2}$, and $nS_{1/2}$–$(n-1)P_{3/2}$ have the largest dipole moments and are good choices for these experiments. Table I shows a few of the possible states for ^{133}Cs and ^{85}Rb that exhibit similar RF transitions. The on-resonant RF transition frequencies are
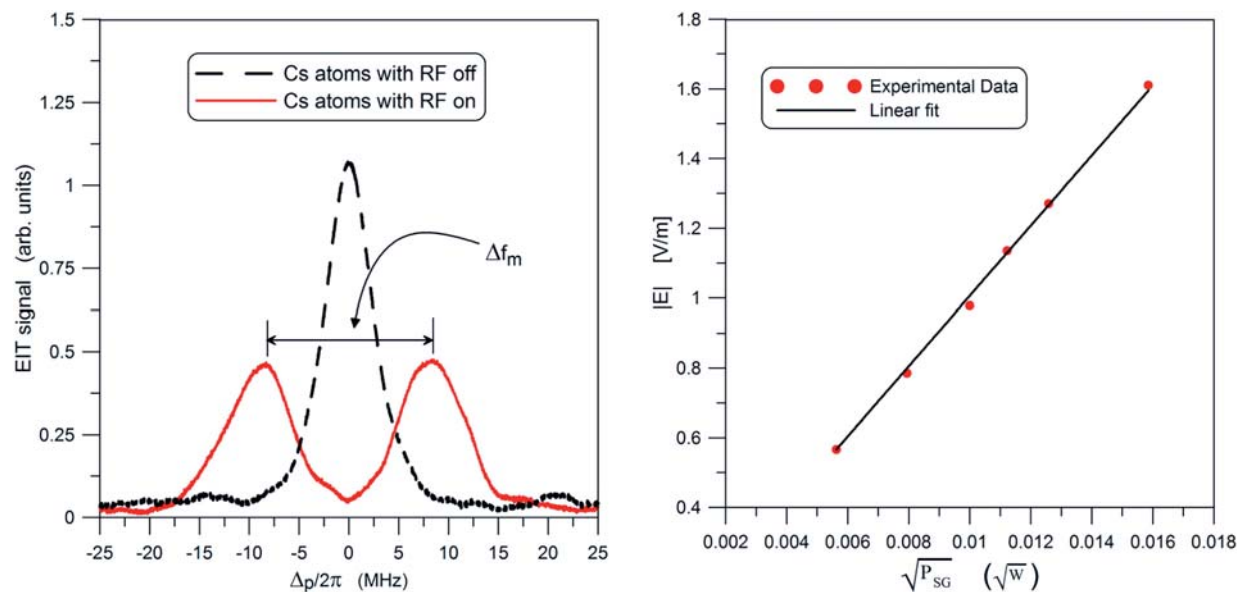

FIG. 2. This dataset is for an RF of 13.404 GHz and corresponds to the following 4-level Cs atomic system: $6S_{1/2} - 6P_{3/2} - 66D_{5/2} - 66P_{3/2}$. (a) Illustration of the EIT signal (i.e., probe laser transmission through the cell) as a function of probe laser detuning Δp. (b) Calculated E-field for a given signal generator power P_{SG}, see discussion below.

TABLE I. RF transitions for ^{133}Cs and ^{85}Rb. In the table, e is the elementary charge and a_o is the Bohr radius.

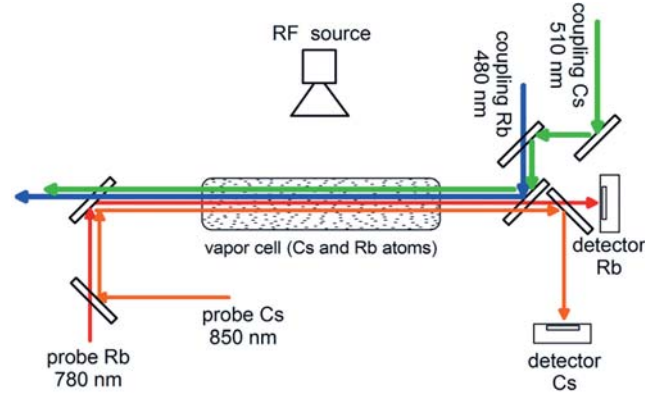|	^{133}Cs states	^{85}Rb states	%f
1	$47D_{5/2} - 48P_{3/2}$	$69D_{5/2} - 68F_{7/2}$	0.09%
	$f_{RF,o} = 6.9458$ GHz	$f_{RF,o} = 6.9571$ GHz	
	$\mathcal{R}_{Cs} = 2946.282\ ea_o$	$\mathcal{R}_{Rb} = 6134.212\ ea_o$	
	$\mathcal{A}_{Cs} = 0.4899$	$\mathcal{A}_{Rb} = 0.4949$	
2	$45D_{5/2} - 46P_{3/2}$	$66D_{5/2} - 65F_{7/2}$	0.16%
	$f_{RF,o} = 7.9752$ GHz	$f_{RF,o} = 7.96823$ GHz	
	$\mathcal{R}_{Cs} = 2687.518\ ea_o$	$\mathcal{R}_{Rb} = 5606.661\ ea_o$	
	$\mathcal{A}_{Cs} = 0.4899$	$\mathcal{A}_{Rb} = 0.4949$	
3	$43D_{5/2} - 44P_{3/2}$	$61D_{5/2} - 62P_{3/2}$	0.01%
	$f_{RF,o} = 9.2186$ GHz	$f_{RF,o} = 9.2264$ GHz	
	$\mathcal{R}_{Cs} = 2440.629\ ea_o$	$\mathcal{R}_{Rb} = 4829.407\ ea_o$	
	$\mathcal{A}_{Cs} = 0.4899$	$\mathcal{A}_{Rb} = 0.4899$	
4	$40D_{5/2} - 41P_{3/2}$	$68S_{1/2} - 68P_{3/2}$	0.33%
	$f_{RF,o} = 11.6187$ GHz	$f_{RF,o} = 11.6665$ GHz	
	$\mathcal{R}_{Cs} = 2092.565\ ea_o$	$\mathcal{R}_{Rb} = 4781.494\ ea_o$	
	$\mathcal{A}_{Cs} = 0.4899$	$\mathcal{A}_{Rb} = 0.4714$	
5	$66S_{1/2} - 66P_{3/2}$	$65S_{1/2} - 65P_{3/2}$	0.20%
	$f_{RF,o} = 13.4078$ GHz	$f_{RF,o} = 13.4398$ GHz	
	$\mathcal{R}_{Cs} = 4360.132\ ea_o$	$\mathcal{R}_{Rb} = 4352.837\ ea_o$	
	$\mathcal{A}_{Cs} = 0.4714$	$\mathcal{A}_{Rb} = 0.4714$	
6	$63S_{1/2} - 63P_{3/2}$	$53D_{5/2} - 52F_{7/2}$	0.26%
	$f_{RF,o} = 15.5513$ GHz	$f_{RF,o} = 15.5924$ GHz	
	$\mathcal{R}_{Cs} = 3951.355\ ea_o$	$\mathcal{R}_{Rb} = 3593.807\ ea_o$	
	$\mathcal{A}_{Cs} = 0.4714$	$\mathcal{A}_{Rb} = 0.4949$	

FIG. 3. Illustration of the vapor cell setup for two atomic species EIT experiments, with counter-propagating probe and coupling beams. The RF is applied transverse to the optical beam propagation in the vapor cell. There are two probe beams (corresponding to Cs and Rb) and two coupling beams (for Cs and Rb) with all four beams overlapping. In the diagram, the beams are separated for clarity; in reality they are all coincident.

denoted as $f_{RF,o}$, which were obtained with the Rydberg formula and the quantum defects for ^{85}Rb and ^{133}Cs.[9–13] Also, in this table are the dipole moments for each state, composed of a radial part $\mathcal{R}$ and an angular part $\mathcal{A}$, where $\wp = \mathcal{R}\mathcal{A}$. The radial part $\mathcal{R}$ is obtained from two numerical calculations (see Ref. [1]) using the quantum defects for ^{85}Rb and ^{133}Cs.[9–13] The angular part of the dipole moment is independent of n; for these four transitions (for $m_j = \pm 1/2$), $\mathcal{A}_{34} = 0.4899$ (for $nD_{5/2}$–$(n+1)P_{3/2}$), $\mathcal{A}_{34} = 0.4949$ (for $nD_{5/2}$–$(n-1)F_{7/2}$), $\mathcal{A}_{34} = 0.4714$ (for $nS_{1/2}$–$nP_{3/2}$), and $\mathcal{A}_{34} = 0.4714$ (for $nS_{1/2}$–$(n-1)P_{3/2}$), see Ref. [14]. Note that these $\mathcal{A}$ correspond to co-linear polarized optical beams and the RF source, which is the case used in these experiments. In this table, we also show the percentage difference in the transition frequencies (%f) between the Cs and Rb states, indicating that these six states have relatively close transition frequencies.

III. DUAL ATOM EXPERIMENTAL SETUP

The experimental setup is shown in Fig. 3. We use a cylindrical glass vapor cell of length 75 mm and diameter 25 mm containing both ^{85}Rb atoms and ^{133}Cs. For the ^{85}Rb atoms, the levels $|1\rangle$, $|2\rangle$, $|3\rangle$, and $|4\rangle$ correspond, respectively, to the ^{85}Rb $5S_{1/2}$ ground state, $5P_{3/2}$ excited state, and two Rydberg states. The probe for ^{85}Rb is a 780.24 nm laser which is scanned across the $5S_{1/2}$–$5P_{3/2}$ transition and is focused to a full-width at half maximum (FWHM) of 80 μm, with a power of 120 nW. To produce an EIT signal in ^{85}Rb, we apply a counter-propagating coupling laser (wavelength $\lambda_c \approx 480$ nm) with a power of 32 mW, focused to an FWHM

of 144 μm. For the ^{133}Cs atoms, the levels $|1\rangle$, $|2\rangle$, $|3\rangle$, and $|4\rangle$ correspond, respectively, to the ^{133}Cs $6S_{1/2}$ ground state, $6P_{3/2}$ excited state, and two Rydberg states. The probe for ^{133}Cs is an 850.53 nm laser which is scanned across the $6S_{1/2}$–$6P_{3/2}$ transition and is focused to a full-width at half maximum (FWHM) of 80 μm, with a power of 120 nW. To produce an EIT signal in ^{133}Cs, we apply a counter-propagating coupling laser (wavelength $\lambda_c \approx 510$ nm) with a power of 32 mW, focused to an FWHM of 144 μm. In order to ensure both Cs and Rb see the same RF field, all four beams are overlapped and focused on to the same spot inside the vapor cell using a bean profiler. We used two different photodetectors (one for the Rb atoms and one for the Cs atoms), allowing us to measure the EIT signal for both atoms separately and simultaneously. We modulate the coupling lasers' amplitude with a 30 kHz square wave and detect any resulting modulation of the probe transmission with a lock-in amplifier. This removes the Doppler background and isolates the EIT signal. The RF E-field at the vapor cell was applied by a signal generator (SG) connected to a horn antenna via an RF cable. The RF power levels (P_{SG}) stated in this paper are the power readings of the SG that feeds the cable which, in turn, feeds the horn antenna. Due to the losses in the feeding cable, the reflections and losses in the horn antenna, and the propagation losses, this is not the power levels (or E-field strengths) incident onto the vapor cell. The E-field strength at the vapor cell is determined by taking into account these various losses.

A. ^{133}Cs: $43D_{5/2}$–$44P_{3/2}$ and ^{85}Rb: $61D_{5/2}$–$62P_{3/2}$

We first performed experiments for an RF transition of approximately 9.22 GHz. From Table I, we see that this transition corresponds to $6S_{1/2}$–$6P_{3/2}$–$43D_{5/2}$–$44P_{3/2}$ for ^{133}Cs and $5S_{1/2}$–$5P_{3/2}$–$61D_{5/2}$–$62P_{3/2}$ for ^{85}Rb. Note that the two atomic species have the same angular momentum states. For the Rb atoms, we used a 479.768 nm coupling laser; for the Cs atoms, we used a 510.018 nm coupling laser. We applied an E-field using a horn antenna placed 318 mm from the vapor cell. Fig. 4 shows a typical simultaneous EIT signal
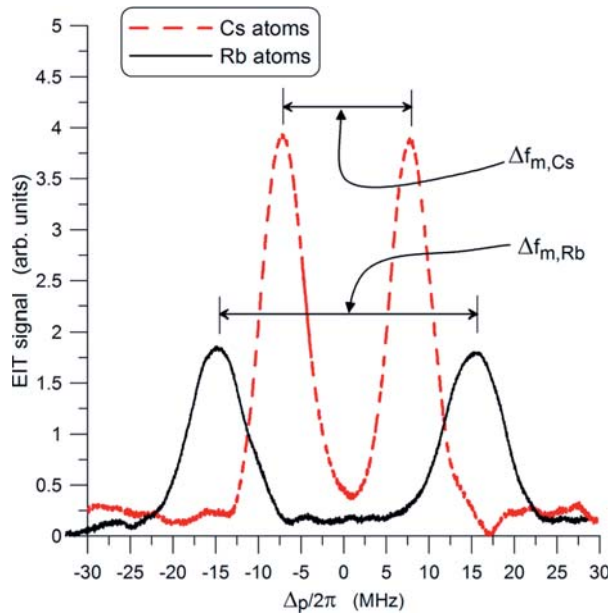
FIG. 4. Illustration of the EIT signal (i.e., probe laser transmissions through the cell) as a function of probe laser detuning Δ_p. The dashed line is the measured EIT signal obtained with the CS atoms and the solid line is the measured EIT signal obtained with the Rb atoms. The observed splitting result from an applied 9.222 GHz RF E-field.

measurement obtained from both the ^{133}Cs and ^{85}Rb atoms for an SG power of -11 dBm and at 9.222 GHz. We see that the measurement splitting (Δf_m) is different for the two atomic species, which is a result of the two atoms having different dipole moments (this is discussed in detail below).

If the RF is detuned from the on-resonant RF transition, the measurement splitting Δf_m (or Δf_o) increases from the on-resonant AT splitting by the following:[15,16]

$$\Delta f_\delta = \sqrt{(\delta_{RF})^2 + (\Delta f_o)^2}, \tag{2}$$

where δ_{RF} is the RF detuning ($\delta_{RF} = f_{RF,o} - f_{RF}$, where $f_{RF,o}$ is the on-resonance RF transition and f_{RF} is the frequency of the RF source) and Δf_o is the separation of the two peaks with no RF detuning (i.e., the on-resonant AT splitting or when $\delta_{RF} = 0$). In order for us to compare measurements for the two different atomic species, we need to correct for the situation where the two species can have slightly different RF transition frequencies. Alternatively, we can assume that the RF source produces the same E-field at the vapor cell for the slightly difference frequencies (within the %f) and then perform on-resonant measurements for each of the two different species. We have verified that the RF source produces constant output power for a given %f, and that the losses in the cable feeding the antenna and the antenna parameters are constant for a given %f. This ensures that the E-field at the vapor cell is constant for a given %f. Therefore, we perform measurements at two slightly different RF frequencies (one at the on-resonant frequency for ^{133}Cs, and one at the on-resonant frequency for ^{85}Rb). With that said, we need to ensure that the two frequencies are indeed at the on-resonant transition for the two atoms. While the data in Table I for $f_{RF,o}$ were calculated from the best current available quantum

defects, there remains the possibility of errors in these quantum defects and in turn errors in the calculation of $f_{RF,o}$. As discussed in Ref. 15, an alternative approach for determining $f_{RF,o}$ is to perform RF detuning experiments and fit the expression in Eq. (2) to a set of measurements for Δf_δ over a range of δ_{RF}. These RF detuning data allow us to determine the on-resonant RF transitions (i.e., $f_{RF,o}$) to within ± 0.25 MHz (determined by averaging several sets of data). This measured $f_{RF,o}$ allows us to make comparisons to calculated values of $f_{RF,o}$ as determined from quantum defects, in effect, assessing the values of the current available quantum defects.

As shown in Eq. (2), a measurement for Δf_o obtained from the off-resonant RF transition frequency will result in an over-estimate of Δf_o and in turn an overestimate $|E|$. Thus, it is important that we determine the on-resonant transition frequencies. To determine these, we performed RF detuning experiments for various RF power levels (P_{SG}) for the two atomic species. The data for Δf_δ for the two atoms are shown in Fig. 5. The data for both atoms were collected simultaneously. Each curve for each atom was fitted to the expression in Eq. (2) and the fitted $f_{RF,o}$ are shown in the figure. Averaging the data for the six different SG power levels, we find that $f_{RF,o} = 9.2184$ GHz for ^{133}Cs and $f_{RF,o} = 9.2269$ GHz for ^{85}Rb. In order to compare these values to those given in Table I (i.e., the ones obtained from the quantum defects), we show vertical lines in Fig. 5 indicating $f_{RF,o}$. For this set of Cs and Rb states, we see that $f_{RF,o}$ obtained from the RF detuning experiments compare very well to those obtained from the calculations using the quantum defects, where the ^{133}Cs results are in better comparison (every so slightly) than the ^{85}Rb results. In the next subsection, we investigate a set of states where we see that there is a significant difference between $f_{RF,o}$ obtained from the calculated and detuning results.

On a side note, there are three papers that give quantum defects for Cs,[11–13] where Refs. 12 and 13 are sequential improvements over those in Ref. 11. If we used the quantum defect data given in Ref. 11, we obtain $f_{RF,o} = 9.2253$ GHz (this frequency is shown in Fig. 5) which is not as close to the measured $f_{RF,o}$ and to those obtained from the new quantum defects.[13] These RF detuning experiments help indicate the accuracy of the very recent quantum defects given in Ref. 13, as well as those for Rb.

With the on-resonant RF transition frequencies now determined, we then perform two sets of measurements for a range of SG power levels (one set for the on-resonant frequency of ^{133}Cs, or $f_{RF,o} = 9.2184$ GHz; one set for the on-resonant frequency of ^{85}Rb, or $f_{RF,o} = 9.2269$ GHz). For the different SG powers, we determine Δf_o for the ^{133}Cs for $f_{RF,o} = 9.2184$ GHz and Δf_o for the ^{85}Rb for $f_{RF,o} = 9.2269$ GHz. These results are shown in Fig. 6. All of these data were collected with all four laser beams propagating through the cell. That is, both atomic species where excited to high Rydberg states. This is further discussed below. From the figure, we notice that the slopes of each curve are different, which are determined by linear fit of the data and are shown in the figure. This is expected because from Eq. (1), the measured splitting for each atom is proportional to $\wp |E|$. As discussed in Ref. 1, this slope can be thought of as the
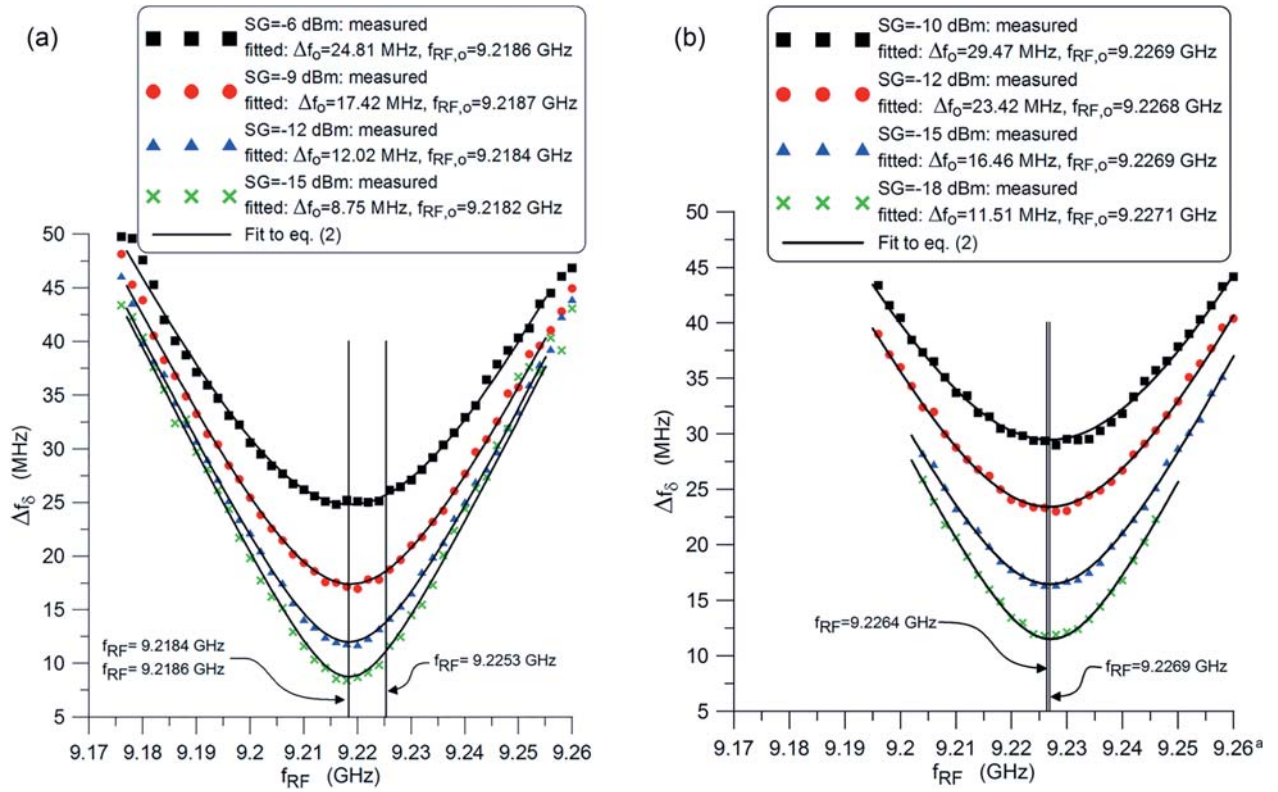
FIG. 5. RF detuning experiments: (a) ^{133}Cs: $43D_{5/2}$-$44P_{3/2}$ and (b) ^{85}Rb: $61D_{5/2}$-$62P_{3/2}$. The vertical lines and corresponding frequencies are the $f_{RF,o}$ obtained from both the RF detuning measurements and from the quantum defect data.

measurement E-field sensitivity for a given atom. Since each atom has a different dipole moment for their respective atomic states, we use (1) to show that the ratio of the slopes for Δf_o (for the same E-field seen by the two atoms) is given by

$$R = \frac{\wp_{Cs}}{\wp_{Rb}} = \frac{\mathcal{R}_{Cs}\mathcal{A}_{Cs}}{\mathcal{R}_{Rb}\mathcal{A}_{Rb}}, \qquad (3)$$
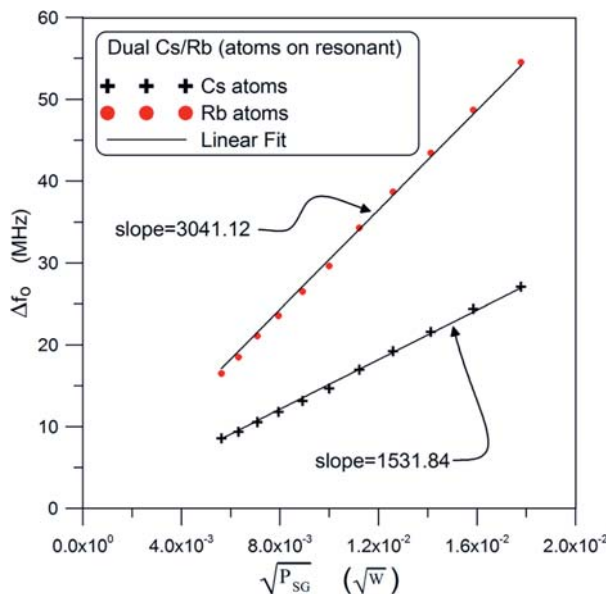

FIG. 6. Δf_o as a function of SG power for the ^{133}Cs at $f_{RF} = 9.218$ GHz and ^{85}Rb at $f_{RF} = 9.227$ GHz.

where R is defined as the "sensitivity ratio" of ^{133}Cs to ^{85}Rb; $\wp_{Cs}$ and $\wp_{Rb}$ are the dipole moments for ^{133}Cs to ^{85}Rb, respectively. The assumption is that the same E-field at the vapor field is generated by the SG source for the two different closely-spaced frequencies (in this case 9.2184 GHz and 9.2269 GHz). This was verified by measuring both the output SG power and the loss in the cable. Using Eq. (3) and the dipole moments given in Table I, we calculated the sensitivity ratio R to be 0.505. Using the data in Fig. 6, we determined the ratio of the slopes from the measurements (1531.84 for ^{133}Cs and 3041.12 for ^{85}Rb) to be 0.504. The difference between the measured and theoretical values of the sensitivity ratio R is 0.1%. This helps confirm that the calculations of the relative dipole moments for the two different atomic species compare well to measurements performed in a thermal cell at room temperature. We have estimated that we can determine the slope of Δf_o to within ±0.4% (determined by averaging several sets of data).

While the difference between the measured and theoretical values of the sensitivity ratio R is small, there are some uncertainties in these measurements. The errors and uncertainties of this measurement approach (including determining Δf_o, the slope of Δf_o, R, and the E-field strength) have contributions from statistical and systematic effects of the measurement itself, along with the validity of the linear relationship between the E-field strength and Δf_o as given by Eq. (1). This linear relationship can breakdown under certain conditions involving the EIT signal linewidth which is a function of the Rabi frequencies of the probe and coupling

lasers.[18] All these effects on the uncertainties of the measurement approach are currently being investigated.

The measured Δf_o for each atomic species was used in Eq. (1) to calculate the E-field at the vapor cell for a range of P_{SG}. These calculated values are given in Fig. 7. The E-field strength obtained from both the ^{133}Cs and ^{85}Rb atoms is the same, illustrating that the two different atomic species can be used simultaneously to independently measure the same E-field strength. For a comparison, we estimated the E-field strength from a far-field calculation. Using P_{SG}, the cable loss (measured to be 2 dB), gain of the horn antenna (estimated to be 14.5 dBi), and the distance of the horn to the vapor ($x = 31.8$ cm), we calculate the E-field in the far-field by[17]

$$|E| = \frac{\sqrt{59.96}}{x}\sqrt{10^{\frac{14.5}{10}} \, 10^{0.001*\frac{(P_{SG}-2)}{10}}}, \qquad (4)$$

where P_{SG} is given in units of dBm. These far-field values are also shown in Fig. 7. The estimated E-field strength obtained for both Cs and Rb shows small deviations from the far field estimates. This illustrates that the two species measurements outperform comparisons based on such calculations.

It is expected that the presence of a second atomic system will not affect the EIT measurements of the first atomic vapor for our given vapor pressures and densities. However, there is the possibility that the two atomic species could interact with each other when they are both excited to high Rydberg state, or one species could possibly act as a buffer gas from the other species perspective.[19] While others have observed interactions between Rb and Cs atoms,[20,21] these are at much higher vapor pressures and densities than in our experiments, and as such, we do not expect to observe any effect on our measurements. To address these possibilities, we performed control experiments. We first repeated the power scan for each atomic species separately. That is, we performed measurements for ^{133}Cs, while the probe and coupling lasers for ^{85}RB were blocked from entering the vapor

cell (^{85}Rb at ground state and ^{133}Cs at a high Rydberg state). Similarly, we performed measurements for ^{85}Rb, while the probe and coupling lasers for ^{133}Cs were blocked from entering the vapor cell (^{133}Cs at ground state and ^{85}Rb at a high Rydberg state). Second, we performed measurements with a pure ^{133}Cs cell and with a pure ^{85}Rb cell. These two cells were the same size as the two species cell. Also, a test fixture was made such that the various cells could be inter-changed while ensuring that the laser beams were always propagating through the cell at the same location. This ensured that the effect for field variability inside the cell[3,7,8] could be controlled and ensured that field was measured at the same location inside each cell. The data from all these different approaches (along with the data from above) are shown in Fig. 8. The data show that all the approaches give the same value of Δf_o and indicate, as expected, that there is no significant interaction between the two different atomic species in the same vapor cell excited to high Rydberg states.

B. ^{133}Cs: $66S_{1/2}$–$66P_{3/2}$ and ^{85}Rb: $65S_{1/2}$–$65P_{3/2}$

We next performed experiments for an RF transition at approximately 13.4 GHz. From Table I, that corresponds to $6S_{1/2}$–$6P_{3/2}$–$66S_{1/2}$–$66P_{3/2}$ for ^{133}Cs and $5S_{1/2}$–$5P_{3/2}$ –$65S_{1/2}$–$65P_{3/2}$ for ^{85}Rb. Note that in this case, the two atomic species have the same angular momentum states, but different angular states for the RF transitions than the previous case. For the Rb atoms, we used a 479.718 nm coupling laser; for the Cs atoms, we used a 509.022 nm coupling laser. We applied an E-field via a horn antenna placed 415 mm from the vapor cell.

Once again, to determine the on-resonant RF transition frequencies, we performed RF detuning measurements. The data from these measurements are shown in Fig. 9. From a fitting of Eq. (2) to these measurements and averaging the data for the different P_{SG}, we find that $f_{RF,o} = 13.4016$ GHz
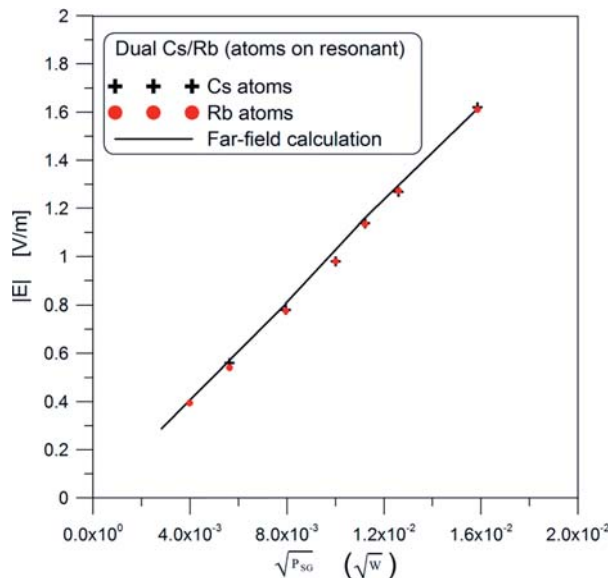
FIG. 7. Calculated $|E|$-field as a function of SG power for the ^{133}Cs at $f_{RF} = 9.218$ GHz and ^{85}Rb at $f_{RF} = 9.227$ GHz.
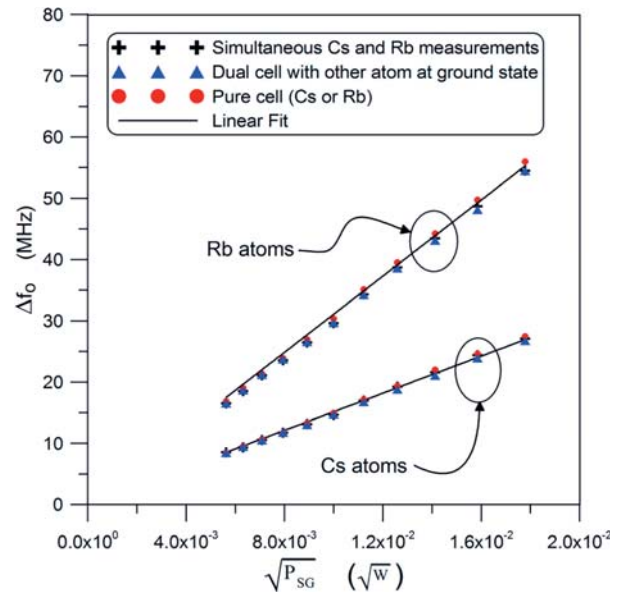
FIG. 8. Comparison of measured Δf_o with dual cell (with both atoms at Rydberg state or for one atom at ground state) and for a pure cell: ^{133}Cs at $f_{RF} = 9.218$ GHz and ^{85}Rb at $f_{RF} = 9.227$ GHz.
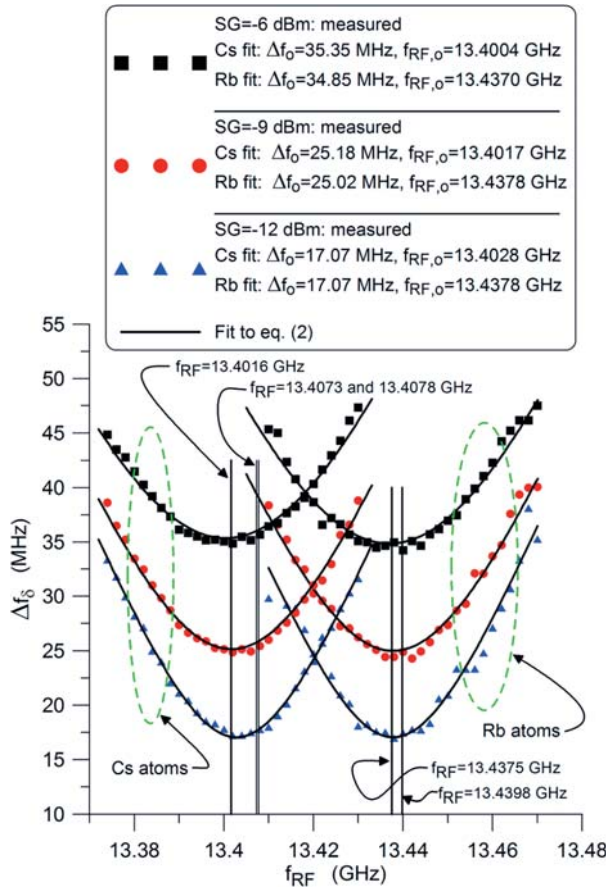
FIG. 9. RF detuning experiments for both ^{133}Cs ($66S_{1/2}$-$66P_{3/2}$) and ^{85}Rb ($65S_{1/2}$-$65P_{3/2}$). The vertical lines and corresponding frequencies are the $f_{RF,o}$ obtained from both the RF detuning measurements and from the quantum defects.

FIG. 10. Δf_o as a function of SG power for the ^{133}Cs at $f_{RF} = 13.4016$ GHz and ^{85}Rb at $f_{RF} = 13.4375$ GHz.

The measured Δf_o for each atomic species was used in Eq. (1) to calculate the E-field at the vapor cell for a range of SG power levels. These calculated values are given in Fig. 11. The estimated E-field strength obtained for both Cs and Rb are the same. We repeated the power scan for each atomic species separately by performing measurements for ^{133}Cs, while the probe and coupling lasers for ^{85}RB were blocked from entering the vapor cell (in effect, ^{85}Rb at ground state and ^{133}Cs at a high Rydberg state). Similarly, we performed measurements for ^{85}Rb, while the probe and

for ^{133}Cs and $f_{RF,o} = 13.4375$ GHz for ^{85}Rb. These values along with the ones given in Table I (calculated from quantum defect data) are shown by vertical lines in Fig. 9. From this figure, we see that the calculated values for $f_{RF,o}$ are different by an appreciable amount. As such, if these calculated values for $f_{RF,o}$ are used for these measurements, then the Δf_o obtained for the off-resonant RF transitions frequency will result in an over-estimate of Δf_o and in turn an overestimate of $|E|$.

With the on-resonant RF transition frequencies determined, we then performed two sets of measurements for a range of P_{SG} (one set for the on-resonant frequency of ^{133}Cs, or $f_{RF,o} = 13.4016$ GHz; one set for the on-resonant frequency of ^{85}Rb, or $f_{RF,o} = 13.4375$ GHz). For the different SG powers, we determine Δf_o for ^{133}Cs at $f_{RF,o} = 13.4016$ GHz and Δf_o for ^{85}Rb at $f_{RF,o} = 13.4375$ GHz. These results are shown in Fig. 10. All the data were collected with all four laser beams propagating through the cell. That is, both atomic species were excited to high Rydberg states. Using the data in Fig. 10, we determined the ratio of the slopes from the measurements (2207.93 for ^{133}Cs and 2189.62 for ^{85}Rb) to be 1.008, and from Eq. (3), the theoretical value for the sensitivity ratio R (using the data in Table I) is 1.002. The difference between the measured and theoretical values of the sensitivity ratio R is 0.6%.
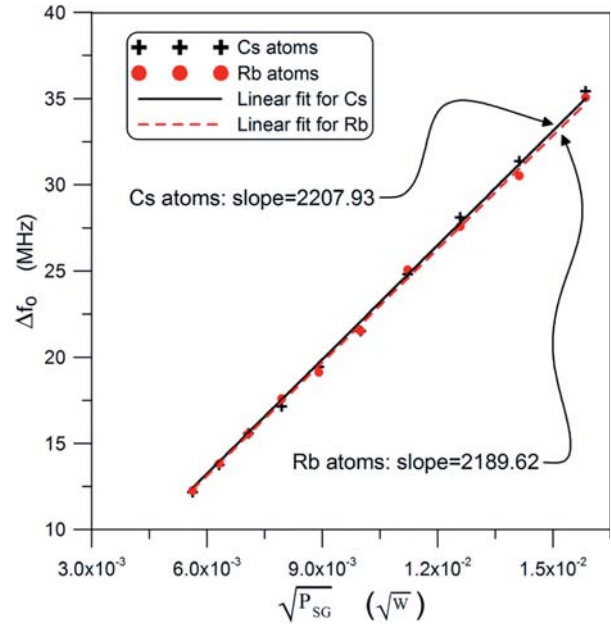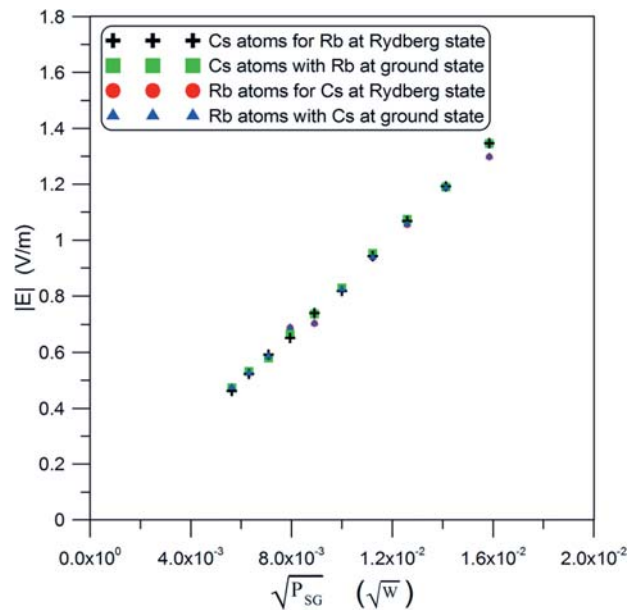

FIG. 11. Calculated $|E|$-field as a function of SG power for the ^{133}Cs at $f_{RF} = 13.4016$ GHz and ^{85}Rb at $f_{RF} = 13.4375$ GHz. Comparison of measured $|E|$-field with both atoms at Rydberg states and for one atom at ground state where no significant systematic atom-atom effects are observed.

coupling lasers for ^{133}Cs were blocked from entering the vapor cell (in effect, ^{133}Cs at ground state and ^{85}Rb at a high Rydberg state). Using these measured Δf_o, we calculated the E-field from Eq. (1) and the results for these single atom measurements are also shown in Fig. 11. The data show that all the approaches give the same value of $|E|$-field and indicate, as expected, that there are no significant interactions between two different atomic species for our vapor pressures and densities.

C. ^{133}Cs: $40D_{5/2}$–$41P_{3/2}$ and ^{85}Rb: $68S_{1/2}$–$68P_{3/2}$

Finally, we performed experiments for an RF transition of approximately 11.6 GHz. From Table I that corresponds to $6S_{1/2}$–$6P_{3/2}$–$40D_{5/2}$–$41P_{3/2}$ for ^{133}Cs and $5S_{1/2}$–$5P_{3/2}$–$68S_{1/2}$–$68P_{3/2}$ for ^{85}Rb. Note that unlike the two previous cases, in this case, the two atomic species have different angular momentum states for the RF transitions. For the Rb atoms, we used a 479.660 nm coupling laser; for the Cs atoms, we used a 510.302 nm coupling laser. We applied an E-field via a horn antenna placed 415 mm from the vapor cell.

Once again, to determine the on-resonant RF transition frequencies, we performed RF detuning measurements. The data are not shown here, but we found that $f_{RF,o} = 11.6172$ GHz for ^{133}Cs and $f_{RF,o} = 11.6656$ GHz for ^{85}Rb. With the on-resonant RF transition frequencies determined, we then performed two sets of measurements for a range of P_{SG} (one set for the on-resonant frequency of ^{133}Cs, or $f_{RF,o} = 11.6172$ GHz; one set for the on-resonant frequency of ^{85}Rb, or $f_{RF,o} = 11.6656$ GHz). These results for the measured Δf_o for various power levels are shown in Fig. 12. All the data were collected with all four laser beams propagating through the cell. That is, both atomic species were excited to high Rydberg states. Using the data in Fig. 12, we determined the ratio of the slopes from the measurements (1067.45 for ^{133}Cs

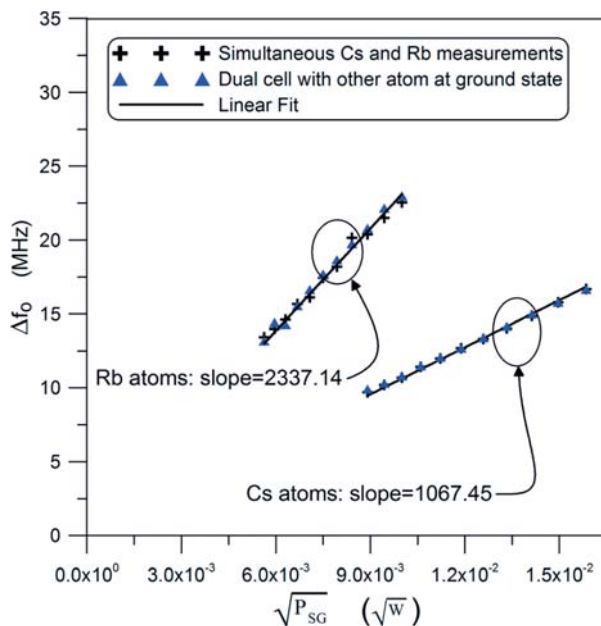and 2337.14 for ^{85}Rb) to be 0.457, and from Eq. (3), the theoretical value of sensitivity ratio R (using the data in Table I) is determined to be 0.455. The difference between the measured and theoretical values of the sensitivity ratio R is 0.4%. This, once again, indicates a good relative comparison between dipole moments for the two different atomic species.

To indicate that there is no significant interaction between each of these two highly-excited Rydberg atoms, we repeated the power scan for each atomic species separately. That is, we performed measurements for ^{133}Cs, while the probe and coupling lasers for ^{85}RB were blocked from entering the vapor cell (^{85}Rb at ground state and ^{133}Cs at a high-Rydberg state). Similarly, we performed measurements for ^{85}Rb, while the probe and coupling lasers for ^{133}Cs were blocked from entering the vapor cell (^{133}Cs at ground state and ^{85}Rb at a high-Rydberg state). These measured Δf_o are also shown in Fig. 13. The data show that all the approaches give the same value for Δf_o.

The measured Δf_o for each atomic species were used in Eq. (1) to calculate the E-field at the vapor cell for a range of P_{SG}. These calculated values are given in Fig. 13. The estimated E-field strength obtained for both Cs and Rb compare well. This illustrates that the two different atomic species can be used simultaneously to independently measure the same E-field strength. Also shown in this figure are the results for the two different atoms at ground states, indicating, as expected, no significant Rydberg atom interactions.

These results for the E-field illustrate the interesting point that using two atomic species simultaneously, one can expand the range of the measurements. Rb atoms have difficulty measuring E-fields for high P_{SG}, and the Cs atoms have difficulty measuring E-fields for lower P_{SG}. For low E-fields strength, it is difficult to measure and/or detect splitting in
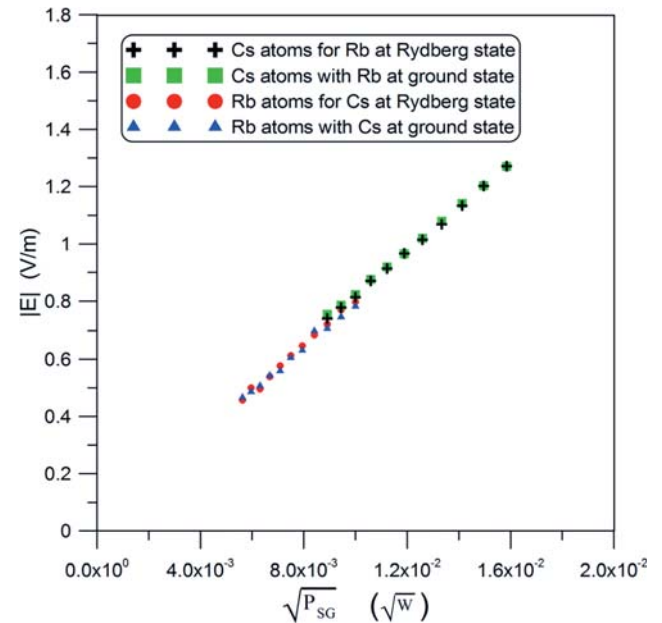

FIG. 12. Δf_o as a function of SG power for the ^{133}Cs at $f_{RF} = 11.6172$ GHz and ^{85}Rb at $f_{RF} = 11.6656$ GHz.

FIG. 13. Calculated $|E|$-field as a function of SG power for the ^{133}Cs at $f_{RF} = 11.6172$ GHz and ^{85}Rb at $f_{RF} = 11.6656$ GHz. Comparison of measured $|E|$-field with both atoms at Rydberg states and for one atom at ground state where no significant systematic atom-atom effects are observed.

the EIT signal. Since the measured Δf_m (or Δf_o) is directly proportional to the product of "$\wp |E|$" (i.e., Eq. (1), when the E-field strength is weak and $\wp$ is small, the ability to measure Δf_m becomes problematic). For this particular set of ^{133}Cs and ^{85}Rb states, the dipole moment for ^{85}Rb is twice as large as the dipole moment for ^{133}Cs, and hence the ^{85}Rb atoms can measure a 50% weaker field. This is evident in Fig. 13 where the smallest field for the ^{133}Cs atoms that can be detected is 0.8 V/m and the smallest field for the ^{85}Rb atoms that can be detected is 0.4 V/m. The maximum detectable field for each atom is limited partially by the methods in which the probe lasers are scanned. We use acoustic-optic modulators (AOMs) to scan the probe laser and as such once AT splitting (i.e., Δf_m) becomes greater than the AOM scan range, an E-field cannot be detected. Since the dipole moment for ^{85}Rb is twice as large as the dipole for ^{133}Cs for this particular set of ^{133}Cs and ^{85}Rb states, the ^{85}Rb atoms will reach this scan limit first, as indicated in the figure.

IV. CONCLUSIONS

In this paper, we demonstrated simultaneous E-field measurement via EIT using both cesium and rubidium in the same vapor cell. Performing such a dual experiment helps quantify various aspects of this type of E-field metrology approach, which are important to understand when establishing an international measurement standard for an E-field strength and is a necessary step for this method to be accepted as a standard calibration technique. For example, these experiments performed in thermal cells at room temperature help in assessing the accuracy in the calculation of the relative dipole moments of the various atoms, where we showed the difference between the measured and theoretical values of the sensitivity ratio R was 0.6% or less for the three cases given here. For the vapor pressures and densities used in our experiments, we do not expect there to be any interactions between the two atomic species when they both are excited to high-Rydberg states. This dual atomic species experiment allows us to confirm this. To address this possibility, we performed a set of experiments in a pure vapor cell, and two separate experiments in a cell with two atomic species. In the separate dual cell experiments, we performed measurements on one atomic species with the probe and coupling lasers for other atomic species blocked from entering the vapor cell (in effect, one atom at ground state and the other at a high-Rydberg state). From these experiments, the two different atomic species appear to not significantly interact when they are both excited to high-Rydberg states (at least for the types of measurements of interest in this paper). Finally, the RF detuning results presented here also help quantify the accuracy of reported quantum defects, which are used in various aspects of these types of measurements.

[1]C. L. Holloway, J. A. Gordon, A. Schwarzkopf, D. A. Anderson, S. A. Miller, N. Thaicharoen, and G. Raithel, IEEE Trans. Antennas Propag. **62**(12), 6169–6182 (2014).

[2]J. A. Sedlacek, A. Schwettmann, H. Kbler, R. Low, T. Pfau, and J. P. Shaffer, Nat. Phys. **8**, 819 (2012).

[3]C. L. Holloway, J. A. Gordon, A. Schwarzkopf, D. A. Anderson, S. A. Miller, N. Thaicharoen, and G. Raithel, Appl. Phys. Lett. **104**, 244102 (2014).

[4]J. A. Gordon, C. L. Holloway, A. Schwarzkopf, D. A. Anderson, S. A. Miller, N. Thaicharoen, and G. Raithel, Appl. Phys. Lett. **105**, 024104 (2014).

[5]J. A. Sedlacek, A. Schwettmann, H. Kbler, and J. P. Shaffer, Phys. Rev. Lett. **111**, 063001 (2013).

[6]A. K. Mohapatra, T. R. Jackson, and C. S. Adams, Phys. Rev. Lett. **98**, 113003 (2007).

[7]C. L. Holloway, J. A. Gordon, M. T. Simons, H. Fan, S. Kumar, J. P. Shaffer, D. A. Anderson, A. Schwarzkopf, S. A. Miller, N. Thaicharoen, and G. Raithel, "Atom-based RF electric field measurements: an initial investigation of the measurement uncertainties," in *EMC 2015: Joint IEEE International Symposium on Electromagnetic Compatibility and EMC Europe*, Dresden, Germany (2015), pp. 467–472.

[8]H. Fan, S. Kumar, J. Sheng, J. P. Shaffer, C. L. Holloway, and J. A. Gordon, Phys. Rev. Appl. **4**, 044015 (2015).

[9]W. Li, I. Mourachko, M. W. Noel, and T. F. Gallagher, Phys. Rev. A **67**, 052502 (2003).

[10]M. Mack, F. Karlewski, H. Hattermann, S. Höckh, F. Jessen, D. Cano, and J. Fortágh, Phys. Rev. A **83**, 052515 (2011).

[11]P. Goy, J. M. Raimond, G. Vitrant, and S. Haroche, Phys. Rev. A **26**(5), 2733–2742 (1982).

[12]K.-H. Weber and C. J. Sansonetti, Phys. Rev. A **35**(11), 4650–4660 (1987).

[13]J. Deiglmayr, H. Herburger, H. Samannshausen, P. Jansen, H. Schmutz, and F. Merkt, Phys. Rev. A **93**, 013424 (2016).

[14]I. I. Sobelman, *Atomic Spectra and Radiative Transitions*, 2nd ed. (Springer, NY, 1996).

[15]M. T. Simons, J. A. Gordon, C. L. Holloway, D. A. Anderson, S. A. Miller, and G. Raithel, Appl. Phys. Lett. **108**, 174101 (2016).

[16]P. R. Berman and V. S. Malinovsky, *Principles of Laser Spectroscopy and Quantum Optics* (Princeton University Press, 2011).

[17]W. L. Stuzman and G. A. Thiele, *Antenna Theory and Design*, 2nd ed. (John Wiley & Sons, Inc., 1998).

[18]H. Zhang, L. Zhang, L. Wang, S. Bao, J. Zhao, and G. Raithel, Phys. Rev. A **90**, 043849 (2014).

[19]A. Sargsyan and D. Sarkisyan, Phys. Rev. A **82**, 045806 (2010).

[20]L. Krause, Appl. Opt. **5**(9), 1375–1382 (1966).

[21]C. Carr, R. Ritter, C. G. Wade, C. S. Adams, and K. J. Weatherill, Phys. Rev. Lett. **111**, 113901 (2013).